



## Pueraria lobata starch regulates gut microbiota and alleviates high-fat high-cholesterol diet induced non-alcoholic fatty liver disease in mice

Yifei Yang<sup>a,b,1</sup>, Mingxing Li<sup>a,b,c,1</sup>, Qin Wang<sup>a,b,1</sup>, Huimin Huang<sup>e</sup>, Yueshui Zhao<sup>a,b,c</sup>, Fukuan Du<sup>a,b,c</sup>, Yu Chen<sup>a,b,c</sup>, Jing Shen<sup>a,b,c</sup>, Haoming Luo<sup>a</sup>, Qianyun Zhao<sup>a</sup>, Jiuping Zeng<sup>a</sup>, Wanping Li<sup>a</sup>, Meijuan Chen<sup>a</sup>, Xiaobing Li<sup>a</sup>, Fang Wang<sup>a</sup>, Yuhong Sun<sup>a</sup>, Li Gu<sup>a</sup>, Zhangang Xiao<sup>d,a,\*</sup>, Xu Wu<sup>a,b,c,\*</sup>

<sup>a</sup> Laboratory of Molecular Pharmacology, Department of Pharmacology, School of Pharmacy, Southwest Medical University, Luzhou, Sichuan, China

<sup>b</sup> Cell Therapy & Cell Drugs of Luzhou Key Laboratory, Luzhou, Sichuan, China

<sup>c</sup> South Sichuan Institute of Translational Medicine, Luzhou, Sichuan, China

<sup>d</sup> Department of Oncology, Affiliated Hospital of Southwest Medical University, Luzhou, Sichuan, China

<sup>e</sup> Jimo District Qingdao Hospital of Traditional Chinese Medicine, Qingdao, Shandong, China

### ARTICLE INFO

#### Keywords:

*Pueraria lobata*  
Starch  
Gut microbiota

### ABSTRACT

The dried roots of *Pueraria lobata* (Willd.) Ohwi as an edible medicinal herb are enriched with starch. However, the structure, physiology, and biological bioactivity of *P. lobata* starch (PLS) has not yet been fully investigated. This study showed that PLS consisted of mixed population of granules with polyhedral or spherical surface. The apparent content of resistant starch was 23.14%, and the molecular weight was  $1.93 \times 10^7$  Da. PLS showed a branching degree and an average polymerization rate of 2.06% and 20.74%, respectively, with fairly high proportion of B1 short chains. The solubility and swelling power of PLS were 38.51% and 28.10 g/g, respectively, showing high hot stability of the viscosity. *In vitro* fermentation of PLS resulted in specifically altered composition of gut microbiota and increased production of SCFAs, showing a potential prebiotic effect. Moreover, PLS remarkably alleviated inflammation, hepatic steatosis and dyslipidemia in mice with high-fat high-cholesterol diet induced non-alcoholic fatty liver disease (NAFLD). The protective effect of PLS was associated with amelioration of NAFLD-associated gut dysbiosis through specifically increasing the abundance of *Lactobacillus*, *Bifidobacterium* and *Turicibacter*, and decreasing *Desulfovibrio*. The results would support the use of PLS as a functional prebiotic for protecting against NAFLD.

### 1. Introduction

The dried root of *Pueraria lobata* (Willd.) Ohwi (Family *Leguminosae*) is an edible food and has long been medicinally used in Asian countries of China, Japan and Korea as a muscle relaxant, antipyretic, anti-dysenteric, as well as for treatment of hypertension (Wong, Li, Li, Rzymowski-Naumovski, & Chan, 2011). Isoflavones, including puerarin,

daidzin, daidzein and their derivatives, are the main bioactive components of *P. lobata* root, which display activities of antioxidant (Wang et al., 2014), anti-inflammation (Jeon, Lee, Lee, & Kim, 2020), anti-tumor (Kapoor, 2013), and anti-diabetes (Chen, Yu, & Shi, 2018). *P. lobata* root is also enriched with starch constituents (Van Hung & Morita, 2007), and only one previous study has shown that a resistant fraction of *P. lobata* starch (PLS) regulated gut microbiota in mice with

**Abbreviations:** ALT, alanine aminotransferase; AST, aspartate aminotransferase; ASV, Amplicon sequence variant; DB, degree of branching; db-RDA, distance-based redundancy analysis; FT-IR, fourier transform infrared spectroscopy; GAM, modified Gifu anaerobic medium; HDL-C, high-density lipoprotein cholesterol; HPAEC, high-performance anion-exchange chromatography; IL, interleukin; LDA, linear discriminant analysis; LDL-C, low-density lipoprotein cholesterol; NAFLD, non-alcoholic fatty liver disease; NMDS, non-metric multidimensional scaling; PCoA, principal coordinates analysis; PLS, *pueraria lobata* starch; RS, resistant starch; SCFA, short chain fatty acid; SEM, scanning electron microscopy; TC, total cholesterol; TG, triglyceride; TNF- $\alpha$ , tumor necrosis factor alpha.

\* Corresponding authors at: Laboratory of Molecular Pharmacology, Department of Pharmacology, School of Pharmacy, Southwest Medical University, Luzhou, Sichuan, China.

E-mail addresses: [xzg555898@hotmail.com](mailto:xzg555898@hotmail.com) (Z. Xiao), [wuxulz@126.com](mailto:wuxulz@126.com) (X. Wu).

<sup>1</sup> These authors contributed equally to this work.

<https://doi.org/10.1016/j.foodres.2022.111401>

Received 17 March 2022; Received in revised form 18 May 2022; Accepted 20 May 2022

Available online 26 May 2022

0963-9969/© 2022 Elsevier Ltd. All rights reserved.

type 2 diabetes mellitus and alleviated hyperglycemia and insulin resistance (Song et al., 2021). However, the interaction between PLS and gut microbiota has not been investigated. Moreover, till now, there is few evidence for the bioactivity of PLS. Therefore, whether PLS could be used as a functional food remains unclear.

Non-alcoholic fatty liver disease (NAFLD) is a liver manifestation of metabolic syndrome, which shows dysregulation of gut-liver axis (Younossi et al., 2016). Gut dysbiosis (the imbalance of gut microbiota) has been proved as one of causes of NAFLD and rectification and alleviation of gut dysbiosis is a proposed strategy to alleviate NAFLD progression (Han, Ma, & Li, 2018; Schnabl & Brenner, 2014). Previous studies have demonstrated that polysaccharides or starches played a role in regulating metabolic syndrome and associated diseases including NAFLD, which had potential to be used as functional food (Yan et al., 2015; Yang et al., 2020; Zhang et al., 2021). Dietary polysaccharides and starch can be degraded by gut microbiota to produce short chain fatty acids (SCFAs), which in turn impact on bacterial balance, and promote intestinal health and energy homeostasis (Hu, Lin, Zheng, & Cheung, 2018; Maslowski & Mackay, 2011). Fermentation of polysaccharides or starch by the gut microbiota may be potentially beneficial to host health and help to protect against metabolic syndrome. Thus, it is of our primary interest to investigate the *in vitro* fermentation of PLS.

Fermentation property of starch is tightly associated with starch structure. In this study, the morphological, structural, and physicochemical characteristics of PLS was first fully investigated. Subsequently, *in vitro* fermentation of PLS was performed to see its impact on gut microbiome and microbial metabolites of SCFAs. The protective effect of PLS against high-fat high-cholesterol diet induced non-alcoholic fatty liver disease was further investigated and evaluated in mice. The results would suggest a prebiotic role of PLS to be used as a functional food.

## 2. Materials and methods

### 2.1. Materials and reagents

Silymarin, rutin and lithium bromide (Li/Br) were obtained from Sigma (USA). Dimethyl sulfoxide (DMSO) was purchased from ANPEL (Shanghai, China). Ultra-pure water was prepared using a Milli-Q water purification system (Millipore, Bedford, USA). Acetic acid, butanoic acid, isobutyric acid, valeric acid, isovaleric acid, hexanoic acid, iso-hexanoic acid and 2-ethylbutyric acid (Purity > 99.0%) were purchased from Sigma (USA). Propanoic acid (Purity > 99.0%) was bought from OKA (Beijing, China). Commercial kits for determination of alanine aminotransferase (ALT), aspartate aminotransferase (AST), total cholesterol (TC), triglyceride (TG), low-density lipoprotein cholesterol (LDL-C), and high-density lipoprotein cholesterol (HDL-C) were bought from Nanjing Jiancheng Bioengineering Institute (Nanjing, China). Mouse tumor necrosis factor alpha (TNF- $\alpha$ ) and interleukin (IL)-6 enzyme-linked immunosorbent assay kits were purchased from R&D System (USA). Modified Gifu anaerobic medium (GAM) was obtained from Hopebio (Qingdao, China). Hematin chloride and vitamin K<sub>1</sub> were provided by Solarbio Co., Ltd (Beijing, China).

### 2.2. Preparation of PLS

The dried roots of *Pueraria lobata* (Willd.) Ohwi were washed with distilled water and sliced into small pieces, which were then milled along with some water in a domestic blender and filtered through 80-mesh sieves. The materials retained in sieves were reprocessed for three times. The resultant fiber residues were discarded, and the resultant liquid fraction were centrifuged at 1500 g at room temperature. The precipitate was resuspended in water and centrifuged again, for three times, which was then washed with ethanol twice and dried at 40 °C. The dried starch was milled and sieved through 80-mesh sieves.

### 2.3. Characterization of PLS

#### 2.3.1. Determination of total flavonoid content

The content of total flavonoids in *P. lobata* starch was conducted using aluminium chloride colorimetric method with rutin used as a standard control as previously described (Yin et al., 2020).

#### 2.3.2. Scanning electron microscopy (SEM)

The morphology of PLS was scanned by a high-resolution field emission SEM (Zeiss Merlin Compact, Germany). The SEM was operated at 5.0 kV and working distance of 20.7 mm. Magnifications at 1000 $\times$  and 2000 $\times$  were used to observe the particle size and surface morphology of starch.

#### 2.3.3. Determination of apparent RS and amylose contents

The resistant starch (RS) content in PLS was determined by the AOAC-GOPOD method as previously reported (Zhang et al., 2021). Amylose content was determined using an iodine colorimetric method as previously reported (Cai et al., 2014). The absorbance was detected at 720 nm by using the Multiskan GO (Thermo, USA).

#### 2.3.4. Molecular size distribution

For molecular size distribution of fully branched starch, starch was thoroughly mixed with 5 mL DMSO solution containing LiBr (0.5% w/w) and heating at 80 °C using a thermomixer for 3 h. The molecular size distribution was analyzed using a SEC-multi-angle laser light scattering detection (MALLS)-refractive index detector (RI) system. The weight- and number-average molecular weight (M<sub>w</sub> and M<sub>n</sub>) and polydispersity index (M<sub>w</sub>/M<sub>n</sub>) of various fractions in DMSO/LiBr (0.5% w/w) solution were measured on a DAWN HELEOS-II laser photometer (He-Ne laser,  $\lambda$  = 663.7 nm, Wyatt Technology Co., Santa Barbara, CA, USA) equipped with three tandem columns (300  $\times$  8 mm, Shodex OH-pak SB-805, 804 and 803; Showa Denko K.K., Tokyo, Japan) which was held at 60 °C using a model column heater. The flow rate was 0.3 mL/min. A differential refractive index detector (Optilab T-rEX, Wyatt Technology Co., Santa Barbara, CA, USA) was simultaneously connected to give the concentration of fractions and the dn/dc value. The dn/dc value of the fractions in DMSO solution was determined to be 0.07 mL/g. The Mark-Houwink parameters for this eluent at 80 °C were  $K = 2.424 \times 10^{-4}$  dL/g and  $\alpha = 0.68$ . RMS Radius (nm) was plotted against detected molar mass (g/mol) to generate RMS conformation plot.

#### 2.3.5. Branching degree

Branching degree of PLS was determined by <sup>1</sup>H NMR (Bruker BioSpin GmbH). An aliquot (10 mg) of starch sample was mixed with 1 mL d<sup>6</sup>-DMSO, and heated at 80 °C overnight, followed by centrifugation at 12,000 rpm for 10 min. Subsequently, the supernatants were added to the nuclear magnetic tube for detection, with a scanning frequency of 32 and a resonant frequency of 500.23 MHz. Branching degree was calculated as follows:

$$\text{Degree of branching (DB) (\%)} = (I-1,6) / (I-1,6 + I-1,4) * 100\% \quad (I-1,6: \alpha-1,6 \text{ glycosidic linkage; } I-1,4: \alpha-1,4 \text{ glycosidic linkage}).$$

#### 2.3.6. Chain-length distributions (CLDs)

PLS (5 mg) was dissolved in 5 mL water in a boiling water bath for 60 min. Sodium azide solution (10  $\mu$ L, 2% w/v), acetate buffer (50  $\mu$ L, 0.6 M, pH 4.4), and isoamylase (10  $\mu$ L, 1400 U) were added to the starch dispersion, and the mixture was incubated in a water bath at 37 °C for 24 h. The hydroxyl groups of the debranched glucans were reduced by treatment with 0.5% (w/v) of sodium borohydride under alkaline conditions for 20 h. The preparation about 600  $\mu$ L was dried in vacuo at room temperature and allowed to dissolve in 20  $\mu$ L of 1 M NaOH for 60 min. Then, the solution was diluted with 580  $\mu$ L of distilled water. The samples were determined by high-performance anion-exchange chromatography (HPAEC) on a CarboPac PA-100 anion-exchange column (4.0  $\times$  250 mm; Dionex) using a pulsed amperometric detector (Dionex

ICS 5000 system).

### 2.3.7. Fourier transform infrared spectroscopy (FT-IR)

FT-IR spectra of PLS was recorded by a Fourier transform infrared spectrometer (Nicolet iZ-10m, Thermo, USA), using the purified potassium bromide piece as the background under the following parameters: 32 scans of every spectrum for average; range, 4000-400  $\text{cm}^{-1}$ ; spectral resolution, 4  $\text{cm}^{-1}$ .

### 2.3.8. Water solubility and swelling power

Water solubility and swelling power of PLS were measured as following method. Firstly, a tube was weighed as M1, and an aqueous suspension of starch (0.01% w/v) in water bath kept at 95 °C for 60 min. Then, the mixture was cooled to room temperature in an ice-bath, followed by centrifugation at 8000 g for 20 min. Subsequently, all supernatants were transferred into a culture dish, which weighed for M2, and the tube with the sediments was weighed as M3. Finally, the supernatants were dried at 100 °C until a constant weight (M4) was obtained. Water solubility and swelling power were calculated as follows:

$W1 = M4 - M2$ ,  $W2 = M3 - M1$ ; Water solubility (%) =  $W1 \div M \times 100\%$ ; Swelling power (g/g) =  $W2 \div (M \times (1-WS))$ ; Where, M is the sample weight (g).

### 2.3.9. Viscous property

The pasting property of PLS was evaluated using a Rapid Visco Analyzer (RVA Super 4, Newport Scientific) according to previous report (Reddy, Luan, & Xu, 2017) with some modification. Viscogram of starch was monitored using starch-water suspensions.

## 2.4. In vitro fermentation of PLS

### 2.4.1. Preparation of fecal slurries

A total of 50 specific-pathogen-free (SPF) male C57BL/6J mice (7-8 weeks) were obtained from Beijing HFK Biotech Co., Ltd. (Beijing, China) and maintained in the animal center of Southwest Medical University. All mice were housed in SPF conditions under a 12-h light/12-h dark cycle with food and water *ad libitum*, which were acclimatized for a week before the start of the experiment. The study was approved by the Southwest Medical University Animal Ethics Committee.

All mice were not treated with any medications before fecal sample collection. Fresh fecal specimens were carefully collected into sterilized tubes and placed on mice. All samples were mixed together. After collection, a total of 5 g of fresh fecal samples were quickly homogenized with anaerobic phosphate-buffered saline (PBS, pH 7.5, containing 0.1% L-cysteine) to prepare 10% (w/v) slurries. Then, the fecal slurries were centrifuged at 500 g for 5 min to remove the food residues, and the suspensions were transported immediately to an anaerobic bag (GasPak EZ Anaerobe Gas Generating Pouch System, BD) for the next batch fermentation assay.

### 2.4.2. Fermentation of PLS

Batch fermentations were conducted under a strict anaerobic environment. The culture system included 18 mL GAM medium supplemented with 5 mg/L vitamin K<sub>1</sub> and 10 mg/L hematin chloride (pH = 7.0), 2 mL fecal suspensions and 50 mg/mL PLS (5% PLS group), which was incubated at 37 °C in an anaerobic pouch. Incubation system without adding 5% PLS served as normal control (NC group). After incubation for 24 or 48 h, samples were taken into an ice-bath for 20 min to stop fermentation. The pH value of culture system after incubation was recorded. An aliquot of samples was centrifuged at 5000 g for 10 min at 4 °C and the resultant bacterial precipitate was used for further microbial analysis via 16S rRNA sequencing. Another aliquot of samples was lyophilized and subjected for determination of short chain fatty acids (SCFAs).

## 2.5. Animal experiments

A total of 24 SPF male C57BL/6J mice (6 weeks,  $22.8 \pm 1.1$  g) were purchased from Beijing HFK Biotech Co., Ltd. (Beijing, China), and housed in the SPF condition ( $23 \pm 2$  °C, 12/12 h light/dark cycles) in animal center of Southwest Medical University. All the mice had free access to food and water. The study was approved by the Southwest Medical University Animal Ethics Committee.

After acclimating for one week, the mice were randomly divided into four groups (n = 6 per group), including ND group as a control group, HFD group, silymarin treatment group as a positive control, and PLS treatment group. The mice in the ND group were fed with normal diet (ND, # LDA0011; Trophic Animal Feed High-Tech Co., Ltd., China) and the other mice were fed with high-fat high-cholesterol diet (HFD, #TP28707, with 20% fat, 1% cholesterol and 0.2% cholate; Trophic Animal Feed High-Tech Co., Ltd., China). The mice in silymarin group were gavaged with 100 mg/kg of the silymarin every other day for 8 consecutive weeks. PLS group were orally treated with 400 mg/kg of gelatinized PLS every day for 8 consecutive weeks. Mice in ND group and HFD group were orally gavaged with distilled water accordingly. Body weight of each mouse was recorded throughout the experiment. On day 56<sup>th</sup>, fresh feces were collected. Mice were anaesthetized for blood collection via cardiac puncture at the end of experiment. Blood samples were further centrifuged after coagulation at 4 °C at sequential 3,000 and 12,000 rpm/min for 5 and 10 min to obtain serum samples, which were stored at -80 °C. Liver tissues and colonic contents were collected for further analysis.

## 2.6. Determination of biochemical indices in serum

The levels of IL-6, TNF- $\alpha$ , ALT, AST, TC, TG, LDL-C and HDL-C in serum were determined by corresponding kits according to the manufacturers' instructions.

## 2.7. H&E, oil red O and Masson's trichrome staining

Formalin-fixed paraffin-embedded liver sections were stained with H & E or Masson trichrome stain as previously reported (Zhu, Xue, Xia, Fu, & Lin, 2017). Frozen liver sections were used for oil red O staining according to previous report (Zhu et al., 2017). Stained sections were inspected using a Nikon Eclipse Ts2R+FL microscope.

Histological score for NAFLD abnormalities ranged from 0 to 12: steatosis (0-3), lobular inflammation (0-3), hepatocellular ballooning (0-3), and fibrosis (0-3).

## 2.8. Bacterial DNA extraction and 16S rRNA sequencing

The bacteria DNA from the *in vitro* fermentation system was extracted using the FastDNA® Spin Kit for soil (MP Biomedicals, USA). Mouse fecal DNA was extracted using the E.Z.N.A.® soil DNA Kit (Omega Biotek, USA). The DNA samples were quality checked and the concentration was quantified by NanoDrop 2000 spectrophotometers (Thermo Fisher Scientific, USA). Polymerase chain reaction (PCR) was conducted to amplify the bacterial 16S rRNA gene fragments (V3-V4) by using primers of 338F (5'-ACTCCTACGGGAGGCAGCAG-3') and 806R (5'-GGACTACHVGGGTWTCTAAT-3'). Illumina MiSeq sequencing was performed through using PE300 chemical at Majorbio Bio-Pharm Technology Co., Ltd. (Shanghai, China). The procedure for sequencing 16S rRNA genes was reported as described in our previous documents (Yin et al., 2020).

Amplicon sequence variants (ASVs) were clustered with 97% similarity cut off. The taxonomy of each 16S rRNA gene sequence was analyzed by Bayes classifier against the Silva (SSU138) 16S rRNA database using confidence threshold of 70%. Sequences were rarefied to the lowest number of sequences per sample before further analysis. Alpha diversity was analyzed using mothur v1.30.1 based on the ASV

level, and beta diversity was determined using QIIME by non-metric multidimensional scaling (NMDS) and principal coordinates analysis (PCoA). Linear discriminant analysis (LDA) was achieved using the LefSe program. Correlation of key microbial changes with main alterations of NAFLD abnormalities was performed by distance-based redundancy analysis (db-RDA) and Pearson's correlation analysis. Analysis of the 16S rRNA microbiome sequencing data was performed using the free online platform of Majorbio Cloud Platform (cloud.majorbio.com).

## 2.9. SCFAs determination

The contents of SCFAs, including acetic acid, propanoic acid,

butanoic acid, iso-butyric acid, valeric acid, isovaleric acid, hexanoic acid and isohexanoic acid, in the fermentation cultures were determined by gas chromatography with mass spectrometry. The assay was performed based on the Agilent 8890B-5977B GC-MSD system (Agilent Technologies Inc., CA, USA), consisting of an electron impact ion source (EI) and an HP-FFAP column (30 m × 0.25 mm × 0.25 μm, Agilent J&W Scientific, USA). The initial column temperature was 80 °C, then increased to 120 °C at 4 °C/min, and increased to 200 °C at 10 °C/min, finally, operating at 230 °C for 3 min. The carrier gas, nitrogen, was set at 1.0 mL/min. Both the temperature of EI source, interface, and quadrupole were set at 230, 230 and 150 °C, respectively, and the scanning mode was ion scanning mode (SIM; electron energy, 70 eV). Injection was performed in split mode at 10: 1 with an injection volume

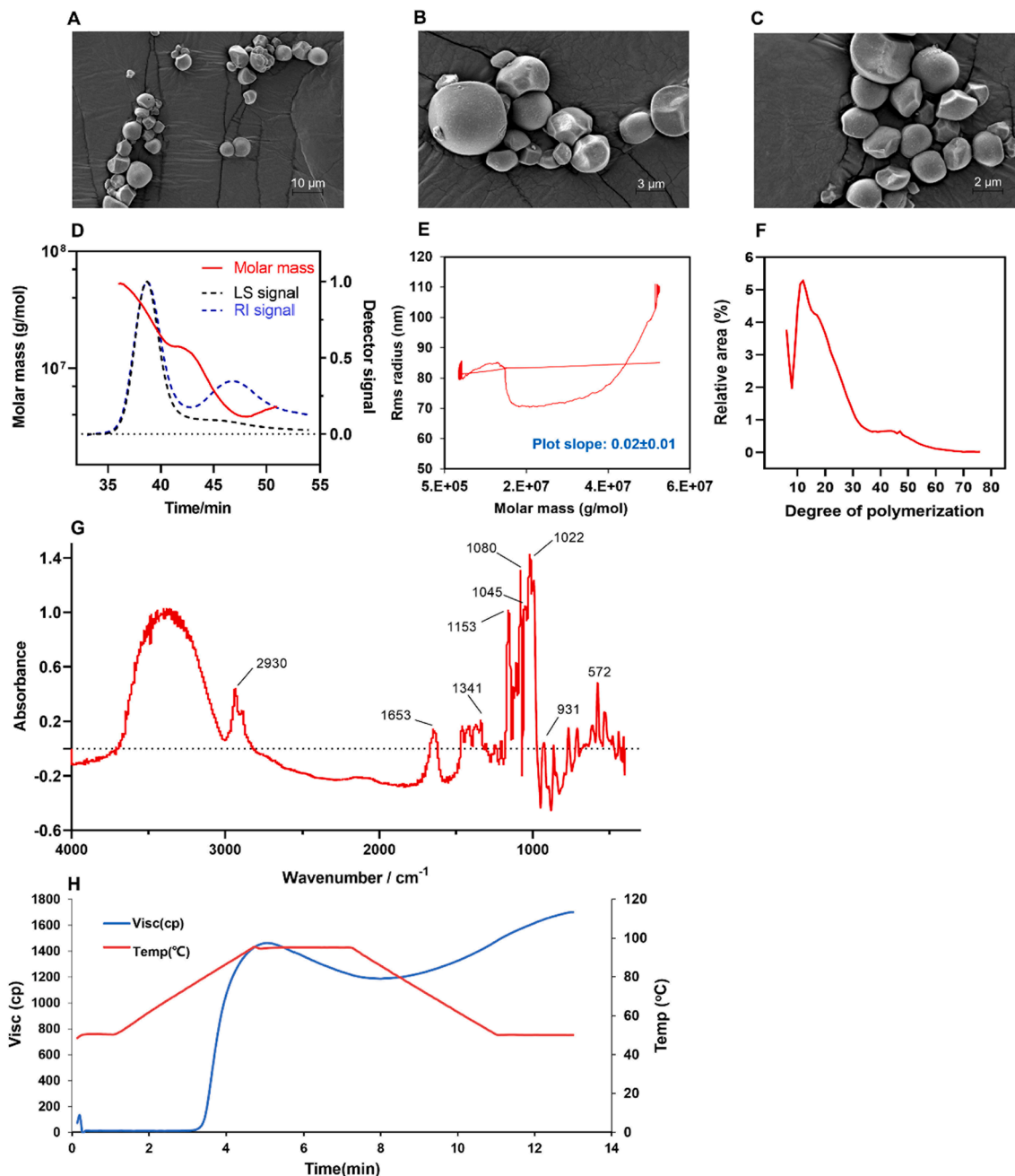


**Fig. 1.** Morphological, structural and physiochemical properties of PLS. (A-C) Micromorphology of PLS by scanning electron microscopy (SEM). (D) Molecular weight distributions of PLS and a representative SEC-MALLS-RI chromatogram. (E) Conformation plot of PLS (via plotting molar mass against rms radius PLS). (F) Chain length distributions (CLDs) of PLS (All CLDs were normalized to the standard oligosaccharides). (G) FT-IR spectra of PLS. (H) Viscosity change during gelatinization.

of 1  $\mu\text{L}$ , with an injector temperature of 260  $^{\circ}\text{C}$ . The details for method validation of each analyte are displayed in supplementary Table 1.

For sample preparation, an aliquot (around 25 mg) of lyophilized fermentation specimen was mixed with 0.5% phosphoric acid (500  $\mu\text{L}$ ) and sonicated (50 Hz) for 10 min at 4  $^{\circ}\text{C}$ , followed by centrifugation at 13,000 g for 15 min at 4  $^{\circ}\text{C}$ . The precipitate was discarded, and the supernatant was vortex mixed with 200  $\mu\text{L}$  n-butanol containing 10  $\mu\text{g}/\text{mL}$  internal standard (2-ethylbutyric acid), followed by sonicated for 10 min at 4  $^{\circ}\text{C}$  and centrifugation at 13,000 g for 5 min at 4  $^{\circ}\text{C}$ . The resultant supernatant was used for analysis.

## 2.10. Statistical analysis

All data were showed as mean  $\pm$  standard deviation (SD). Unpaired student's *t* test and one-way ANOVA analysis with Tukey's test was used to determine the statistical difference by using the software of GraphPad Prism 6 (USA). All the results' significance was determined based on  $p < 0.05$ .

## 3. Results and discussion

### 3.1. Structural and physicochemical characterization of PLS

#### 3.1.1. Morphological structure

The micromorphology of PLS granules was observed using SEM (Fig. 1A-C). PLS consisted of mixed populations of different sizes of granules. Some of PLS was polyhedral or irregular in shape, and some were spherical or ellipsoidal. The results were consistent with previous report (Chen et al., 2017). The surfaces of most PLS were smooth and in relatively loose structure, with some of PLS showing rough, concave and convex surface. This may be attributed to the presence of RS fractions in PLS (Zeng et al., 2019).

#### 3.1.2. Apparent RS and amylose content

The results showed that the apparent RS and amylose contents in PLS were determined as 23.14  $\pm$  0.36% and 20.58  $\pm$  0.20%, respectively. In general, the RS content of granular starch was directly proportional to amylose content (Sang, Bean, Seib, Pedersen, & Shi, 2008; Shi, Chen, Yu, & Gao, 2013). It is suggested that PLS naturally contained considerable fraction of RS.

#### 3.1.3. Molecular weight distribution

Molecular weight distribution of PLS was conducted on SEC-MALLS-RI, with chromatogram displayed in Fig. 1D. Molecular parameters of PLS were then calculated, including molecular weight (Mn, Mw, Mz and Mp), polydispersity index, and rms radius moments. Mw/Mn and Mz/Mn ratio as the polydispersity index shows molecular weight distribution of starch. As shown in Table 1, the values for PLS including Mn, Mw, Mz and Mp were 9.28 $\times 10^6$ , 1.93 $\times 10^7$ , 2.93 $\times 10^7$  and 2.94 $\times 10^7$  Da, respectively, with polydispersity (Mw/Mn and Mz/Mn) value of 2.08  $\pm$

**Table 1**  
Molecular parameters of PLS. (n = 3).

Molecular characteristics	Parameter	Results
Molar mass moments (g/mol)	Mn	(9.28 $\pm$ 0.51) $\times 10^6$
	Mp	(2.94 $\pm$ 0.0058) $\times 10^7$
	Mw	(1.93 $\pm$ 0.041) $\times 10^7$
	Mz	(2.93 $\pm$ 0.023) $\times 10^7$
Polydispersity	Mw/Mn	2.08 $\pm$ 0.07
	Mz/Mn	2.97 $\pm$ 0.35
Rms radius moments (nm)	Rn	80.3 $\pm$ 0.14
	Rw	78.15 $\pm$ 0.64
	Rz	77.55 $\pm$ 1.20

Note: Mn, number-average molecular weight; Mp, peak molecular weight; Mw, weight-average molecular weight; Mz, z-average molecular weight. Rn, number-average radius; Rw, weight-average radius; Rz, z-average radius.

0.07 and 2.97  $\pm$  0.35. The Rn, Rw and Rz of PLS were 80.3  $\pm$  0.14, 78.15  $\pm$  0.64 and 77.55  $\pm$  1.20, respectively.

The conformation plot (via plotting molar mass against rms radius) of PLS is displayed in Fig. 1E. It has been suggested that the conformation plot slope could be used as a reference for molecular configuration. Slope value about 1 shows that the molecule is rod-shaped, slope near to 0.5-0.6 means irregular line cluster and slope as 1/3 means spherical. The plot slope of PLS was around 0.02, which indicated that PLS molecular particles were generally spherical.

#### 3.1.4. Branching degree and chain-length distributions (CLDs) of PLS

The branching extent of PLS was further investigated by  $^1\text{H}$  NMR. The branching degree of PLS as the ratio of  $\alpha$ -1,6 and  $\alpha$ -1,4 glycosidic linkages was 2.06  $\pm$  0.02%. It is suggested that PLS showed a low-to-medium level of branching degree.

A relatively proper DP with a range of 10 to 100 was desirable for the formation of double helices and crystallization (Eerlingen et al., 1993; Gidley et al., 1995). The CLDs of PLS amylopectin with a DP range of 6 to 76 mainly was thus further analyzed (Fig. 1F). The PLS amylopectin exhibited trough levels at DP8, two peaks at DP 11-13 and at around DP 42, and a shoulder at DP 18 (Fig. 1F). The amylopectin chain length distribution was classified as A chains (DP 6-12), B1 chains (DP 13-24), B2 chains (DP 25-36) and B3 chains (DP  $\geq$  37) (Hanashiro, Abe, & Hizukuri, 1996). Table 2 presents the summary of debranched chain length distribution of PLS. The results showed that PLS had an average polymerization of 20.74%, with a relative high proportion of B1 chains (46.1%), followed by A chains (26.5%). The A chains were short external chains which was further divided into very short (DP 6-8) and short (DP 9-12) chains. The very short chains are known as the fingerprint region as it is specific for botanical source. The ratio between short (DP 9-12, S<sub>A</sub>F) and long (DP 13-24, LF) chains (S<sub>A</sub>F/LF ratio) was then calculated to characterize PLS. The S<sub>A</sub>F/LF ratio of PLS was 0.39  $\pm$  0.013, indicating a relative high proportion of long chains. Previous study showed that crystalline B-type and C-type starches including the high amylose corn starch, potato starch, waxy potato starch, wrinkled pea starch and green pea starch (S<sub>A</sub>F/LF, 0.40-0.43) contained higher amounts of long chains than the A-type of corn starch and waxy corn starch (S<sub>A</sub>F/LF, 0.48-0.52) (Gaenssle, Satyawati, Xiang, van der Maarel, & Jurak, 2021). The data of PLS (S<sub>A</sub>F/LF, 0.39  $\pm$  0.013) suggested that PLS may be B-type or C-type starch.

#### 3.1.5. FT-IR analysis

FT-IR is a sensitively effective method for detecting the ordered structure of starch granules. The FT-IR spectrum of PLS is displayed in Fig. 1G. The absorption bands at 1045, 1022 and 995  $\text{cm}^{-1}$  are characteristic absorption of starch structure. The absorption peak at 1045  $\text{cm}^{-1}$  was the structural characteristic of starch crystallization region, which corresponded to the ordered structure of starch aggregation structure. The absorption peak at 1022  $\text{cm}^{-1}$  was the structural characteristic of starch amorphous region, which represented the random line cluster structure of starch macromolecule. The absorption peak at 995  $\text{cm}^{-1}$  was mainly caused by the bending vibration of C-OH, which was attributed to the hydrogen bond structure formed between hydroxyl groups of starch macromolecules (Sevenou, Hill, Farhat, & Mitchell, 2002; Smits, Ruhnau, Vliegenthart, & van Soest, 1998). The absorbance ratios of 1022/995  $\text{cm}^{-1}$  and 1045/1022  $\text{cm}^{-1}$  were used to measure the

**Table 2**  
Summary of debranched chain length distribution of PLS. (n = 3).

Relative area (%)				Average polymerization (%)
DP 6-12	DP 13-24	DP 25-36	DP >37	
26.5 $\pm$ 0.71	46.1 $\pm$ 1.43	15.9 $\pm$ 0.76	11.5 $\pm$ 1.39	20.74 $\pm$ 0.55

Note: Percentages of areas were calculated as the respective fraction areas divided by the total area under the curve.

proportion of amorphous to ordered starch structure and to quantify the order degree of starch granules, respectively, with a higher ratio indicating a higher fraction of crystalline region (Ma & Boye, 2018; Sevenou et al., 2002). As shown in the Table 3, the PLS showed evidently strong reflections at 995, 1022 and 1045  $\text{cm}^{-1}$ , and the ratios of 1022/995 $\text{cm}^{-1}$  and 1045/1022  $\text{cm}^{-1}$  were 1.12 and 0.75, respectively, which indicated an appropriate degree of crystallinity in PLS granules.

### 3.1.6. Water solubility and swelling power

The water solubility and swelling power could be used to evaluate the interaction between starch chains and granules, expressly within the amorphous and crystalline regions (Singh, Inouchi, & Nishinari, 2006). Previous studies have reported that the water solubility and swelling power of starch would be elevated with the increase of temperature, while RS showed prefer stability than natural starch at high temperature, due to the double helix structure of RS could enhance the interaction between starch chains and particles at the amorphous and crystal region, and prevent fracturing the hydrogen bond to release short starch (Genkina, Wikman, Bertoft, & Yuryev, 2007; Zhang et al., 2021). The solubility and swelling power of PLS were determined as  $38.51 \pm 0.71\%$  and  $28.10 \pm 0.68 \text{ g/g}$ , respectively, which indicated the RS component of PLS has a good effect on maintaining the whole crystalline structure.

### 3.1.7. Pasting property

Subsequently, the pasting property of PLS was investigated. A plot of paste viscosity along the temperature change during gelatinization was recorded (Fig. 1H). The pasting profile of PLS including peak viscosity, trough viscosity, breakdown, final viscosity, setback, peak time and pasting temperature is summarized in Table 4. The peak viscosity was an index of starch granules resistant to the swelling and begin to be distorted since it could not hold water any more (Zhong, Li, Ibáñez, Oh, McKenzie, & Shoemaker, 2009). Disruption of starch granules leads to a reduction of paste viscosity which is termed as trough viscosity and the difference between peak and trough viscosity is the breakdown viscosity. Breakdown viscosity reflected paste stability. The swollen starch granules during cooling would result in an increased viscosity that was called setback viscosity. Pasting temperature is the temperature at which the viscosity begins to increase during the heating process. The results showed that PLS did not display a high peak viscosity, which may be due to the presence of B type starch, as A type starch with larger granule size could lead to a higher peak viscosity. We also observed a relative low breakdown value and high setback of PLS, which demonstrated a high hot stability of the viscosity and a strong degree of recrystallization of the gelatinized PLS during cooling.

## 3.2. In vitro fermentation of PLS

### 3.2.1. Regulation of gut microbiota by PLS

Gut microbiome are the core player to degrade polysaccharides including resistant starch, resulting in the increase of dietary polysaccharide fermented as SCFAs (Lozupone et al., 2008). At the meanwhile, the polysaccharides in turn can act as a primary source of carbon and energy for gut microbial community (Lozupone et al., 2008). Notably, different sources of polysaccharides may distinctly impact on gut microbial compositions. Thus, in this study, the effect of PLS (5%, w/v) on regulation of gut microbiota composition was assessed by 16S rRNA sequencing after fermentation.

**Table 3**

IR ratios of the absorbance (1022/995)  $\text{cm}^{-1}$  and (1045/1022)  $\text{cm}^{-1}$  for deconvoluted FT-IR spectra of PLS. (n = 3).

Relative absorbance			IR ratio	
995 $\text{cm}^{-1}$	1022 $\text{cm}^{-1}$	1045 $\text{cm}^{-1}$	(1022/995)	(1045/1022)
1.23 $\pm$ 0.03	1.37 $\pm$ 0.05	1.03 $\pm$ 0.01	1.12 $\pm$ 0.02	0.75 $\pm$ 0.02

**Table 4**

Pasting profiles of PLS. (n = 3).

Pasting profiles	Values
Peak viscosity (cp)	1475.00 $\pm$ 15.63
Trough viscosity (cp)	1176.00 $\pm$ 39.83
Breakdown viscosity (cp)	299.70 $\pm$ 35.92
Final viscosity (cp)	1701.00 $\pm$ 38.53
Setback viscosity (cp)	525.00 $\pm$ 9.54
Peak time (min)	5.05 $\pm$ 0.04
Pasting temperature ( $^{\circ}\text{C}$ )	77.90 $\pm$ 0.48

NMDS analysis at ASV level showed an apparently different microbial structure between NC and 5% PLS group, as the samples in each group were well separated (Fig. 2A). At phylum level (Fig. 2B), Firmicutes and Proteobacteria were the dominant phylum. Compared with the normal control group, the Firmicutes in the 5% PLS group were significantly increased ( $p < 0.01$ ) from 73.83% to 94.55%, however, the level of Proteobacteria was significantly decreased ( $p < 0.01$ ) from 25.01% to 5.02%. Furthermore, at genus level, fermentation with 5% PLS significantly promoted ( $p < 0.001$ ) growth of *Lactobacillus* (Fig. 2C) while significantly inhibited ( $p < 0.05$ ) *Escherichia-Shigella*, *Enterococcus* and *Desulfovibrio* (Fig. 2D-F).

*P. lobata* root is rich in isoflavones such as daidzin, daidzein and puerarin. Previous study has also reported that isoflavones had a modulatory role on gut microbiota. Since the flavonoid content in PLS was determined to be very low (0.25  $\pm$  0.02 mg/g), it is evident that the regulation of PLS on gut microbiota was attributed to the starch constituents.

It has been reported that *Lactobacillus* promotes health functions via attenuating inflammation and maintaining gut homeostasis. In addition, increased Proteobacteria was a signature of gut dysbiosis and a risk index of Crohn's disease (Shin, Whon, & Bae, 2015; Vester-Andersen et al., 2019). *Escherichia-Shigella* and *Enterococcus* have been reported as opportunistic pathogenic bacteria (Jung, Chen, Suyemoto, Barnes, & Borst, 2018; Xu et al., 2018). *Desulfovibrio* (Proteobacteria) could generate the potentially toxic substance of hydrogen sulfide, contributing to gut inflammation (Carbonero, Benefiel, Alizadeh-Ghamsari, & Gaskins, 2012; Mukhopadhyaya, Hansen, El-Omar, & Hold, 2012). The results herein demonstrated that PLS supplementation may have a beneficial effect on the gut health potentially through elevating beneficial bacteria and declining opportunistic harmful bacteria.

### 3.2.2. pH shift of the fermentation

Next, we determined the pH value of culture system during fermentation. As shown in Fig. 2G, after incubation for either 24 h or 48 h, the pH value in GAM + 5% PLS group was significantly lower ( $p < 0.05$ ) than that in the GAM group. The decreased pH in the polysaccharides-fermentation was observed with some reported literatures (Broekaert et al., 2011), which may be associated with the generation of fermented products such as SCFAs.

### 3.2.3. SCFAs production

SCFAs are volatile fatty acids with 2-6 carbon atoms which were produced by gut microbiota as the major products of polysaccharide fermentation, and are important to maintain the normal function of the large intestine (Ríos-Covián et al., 2016; Smith et al., 2013). Moreover, SCFAs play a role in reducing the risk of type 2 diabetes, inflammatory bowel diseases and improving colonocyte health (Sonnenburg et al., 2010; Wang et al., 2020). To see whether fermentation of PLS promotes SCFA production, the SCFA contents were then determined.

As shown in Fig. 2H, after 48 h of fermentation, compared to the NC group, the contents of acetic acid, butyric acid, valeric acid, isovaleric acid and hexanoic acid were significantly higher in the 5% PLS group ( $p < 0.05$ ). As a result, formation of total SCFAs were significantly increased ( $p < 0.05$ ).

SCFAs play an important role in maintaining gut health and

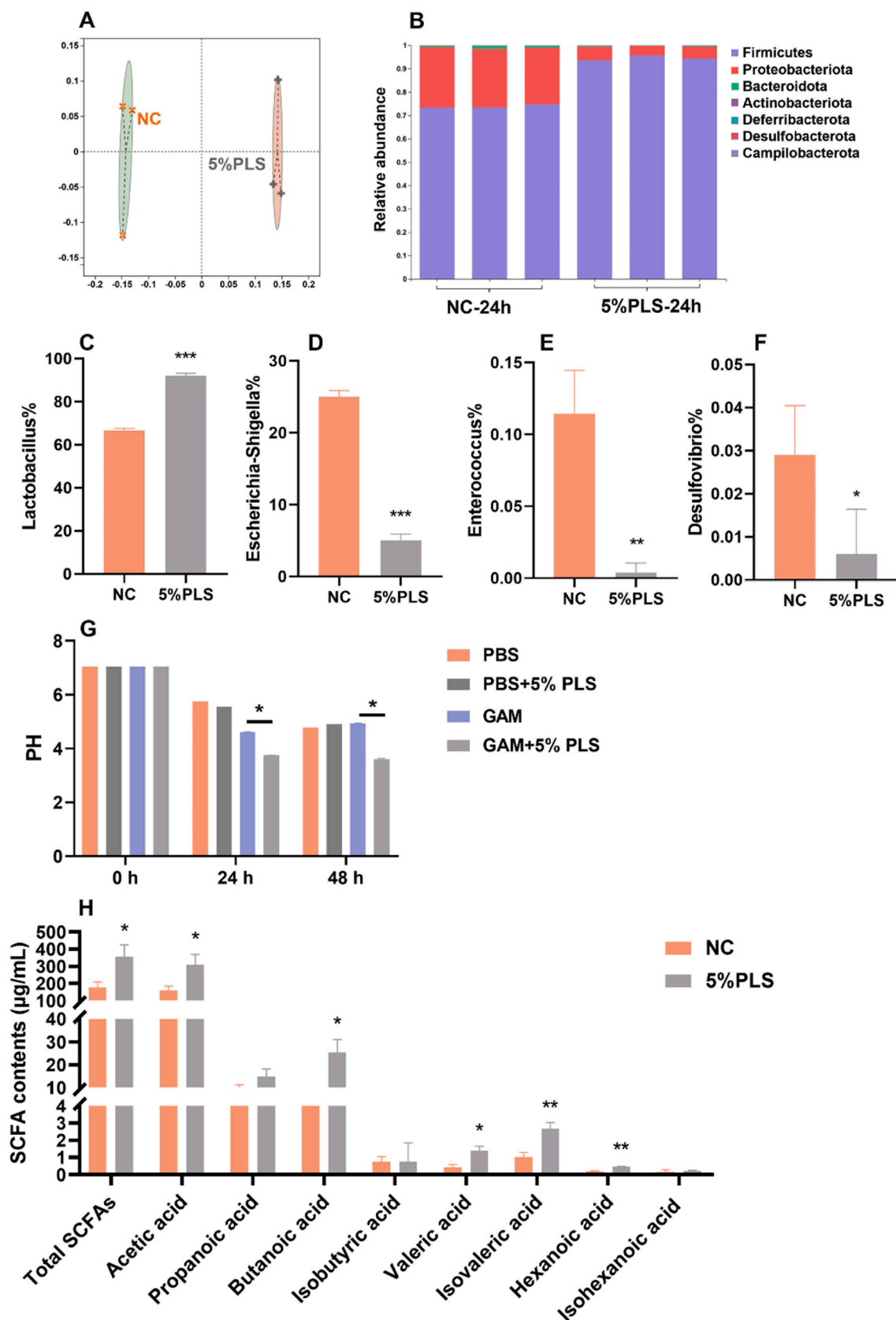


Fig. 2. *In vitro* fermentation of PLS with mouse fecal microbiota under anaerobic condition. (A) NMDS analysis based on ASV level. (B) Community abundance on phylum level. (C) Relative abundance of *Lactobacillus*. (D) Relative abundance of *Escherichia-Shigella*. (E) Relative abundance of *Enterococcus*. (F) Relative abundance of *Desulfovibrio*. (G) PH values alteration in fermented cultures. (H) SCFAs production after fermentation. NC, fermented cultures in the absence of 5% PLS solution. 5% PLS, fermented cultures in the presence of 5% PLS solution. \*  $p < 0.05$ , \*\*\*  $p < 0.001$ , vs NC group.

prevention of certain diseases. For example, butyrate as a major nutrient of the colonocytes, which have been related to promote colonic health and reduce the chances of colorectal cancer (Keku, Dulal, Deveaux, Jovov, & Han, 2015). Thus, PLS fermentation in colon may have a potential prebiotic function.

### 3.3. PLS supplementation alleviated NAFLD in mice

#### 3.3.1. PLS attenuated systemic inflammation

The details for experimental design are displayed in Fig. 3A. From the morphology picture of liver (Fig. 3B), liver of HFD mice was much whiter than that of ND mice, indicating hepatic fat accumulation. After treatment with silymarin and PLS, the HFD liver became ruddy (Fig. 3B). The PLS seemed to display a better effect compared to the silymarin.

Compared to ND mice, HFD diet led to a slight weight gain during week 6<sup>th</sup> to 8<sup>th</sup> (Fig. 3C). PLS administration significantly reduced body weight of HFD mice, while silymarin had a minimal effect (Fig. 3C). Moreover, the inflammatory levels of IL-6 and TNF- $\alpha$  were detected (Fig. 3D-E). Compared to the ND group, the levels of IL-6 and TNF- $\alpha$  were significantly increased ( $p < 0.001$ ) in HFD group. Notably, both silymarin and PLS treatment significantly attenuated inflammation in HFD mice ( $p < 0.001$ ).

The results showed that PLS reduced body weight and attenuated inflammatory factors of HFD mice.

#### 3.3.2. PLS alleviated liver steatosis and dyslipidemia in HFD-induced NAFLD

To further confirm the protective effect of PLS in NAFLD mice, histological examination of liver sections and determination of biochemical indices were conducted.

Compared to the ND group, H&E staining showed that there were more infiltrated inflammatory cells and visible fat vacuoles in the HFD group. Oil red O staining presented that there were a large number of lipid droplets stained by red in the HFD group, and Masson staining exhibited obvious mild fibrosis in the HFD group. Notably, histology score was significantly increased in HFD mice based on the H&E, Oil Red O and Masson's trichrome staining (Fig. 4D). Meanwhile, HFD-induced NAFLD mice was verified by elevating the levels of serum ALT ( $p < 0.01$ ), AST ( $p > 0.05$ ), TC ( $p < 0.001$ ), TG ( $p < 0.001$ ) and LDL-C ( $p < 0.001$ ) (Fig. 4E-I), along with decreased serum HDL-C level ( $p < 0.001$ ) (Fig. 4J).

Compared to HFD group, PLS treatment remarkably attenuated HFD-induced hepatic ballooning, inflammatory infiltration, lipid accumulation and fibrosis, showing decreased histological scores ( $p < 0.001$ ) (Fig. 4A-D). Moreover, PLS significantly reduced HFD-mediated upregulation of serum ALT, AST, TC, TG and LDL-C, while it had no effect on HDL-C level (Fig. 4E-J). Notably, the protective effects of PLS against NAFLD was similar to that of silymarin.

Taken together, PLS improved liver abnormalities and suppressed HFD-induced development of NAFLD via inhibiting de novo lipid lipogenesis, fat accumulation and liver injury.

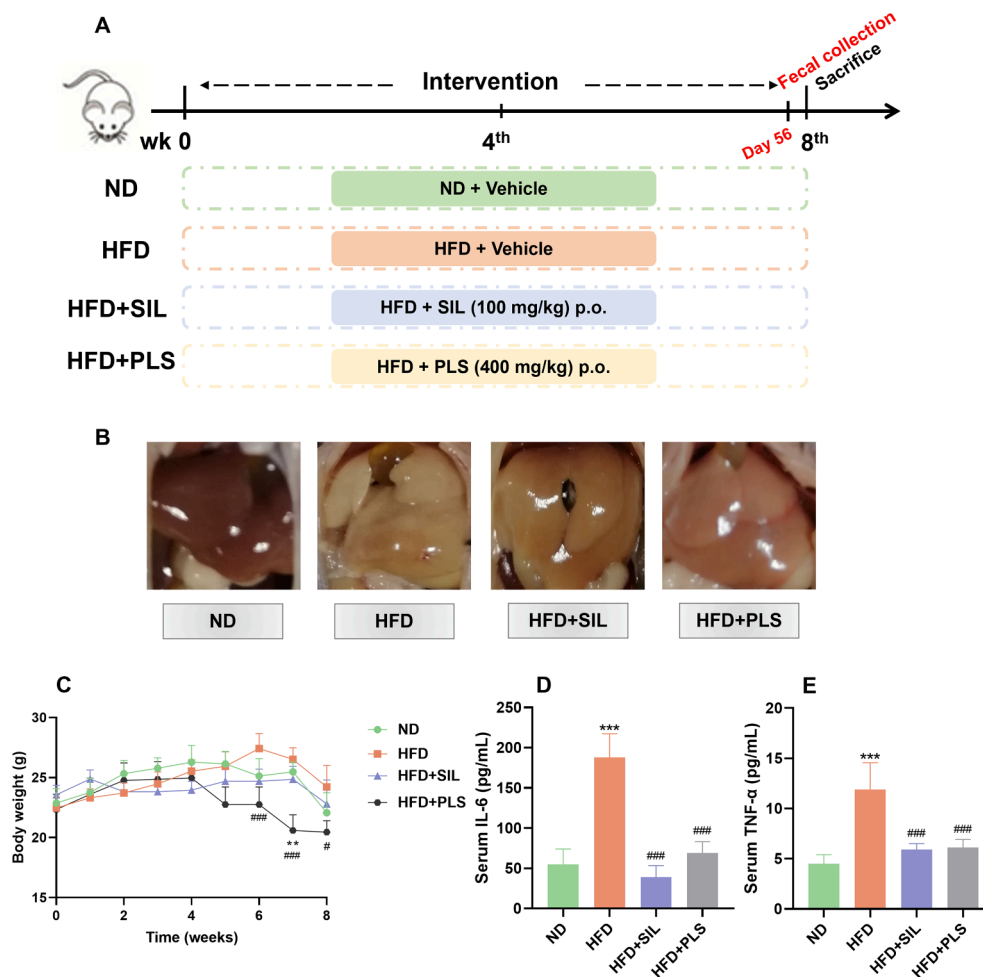


**Fig. 3.** PLS alleviated systemic inflammation in HFD-induced NAFLD. (A) Experimental design of study. (B) Representative morphology images of mouse livers after treatment. (C) Weekly body weight changes of mice. (D) Serum level of IL-6. (E) Serum level of TNF- $\alpha$ . \*\*  $p < 0.05$ , \*\*\*  $p < 0.001$ , vs. ND group; ##  $p < 0.01$ , ###  $p < 0.001$  vs HFD group.

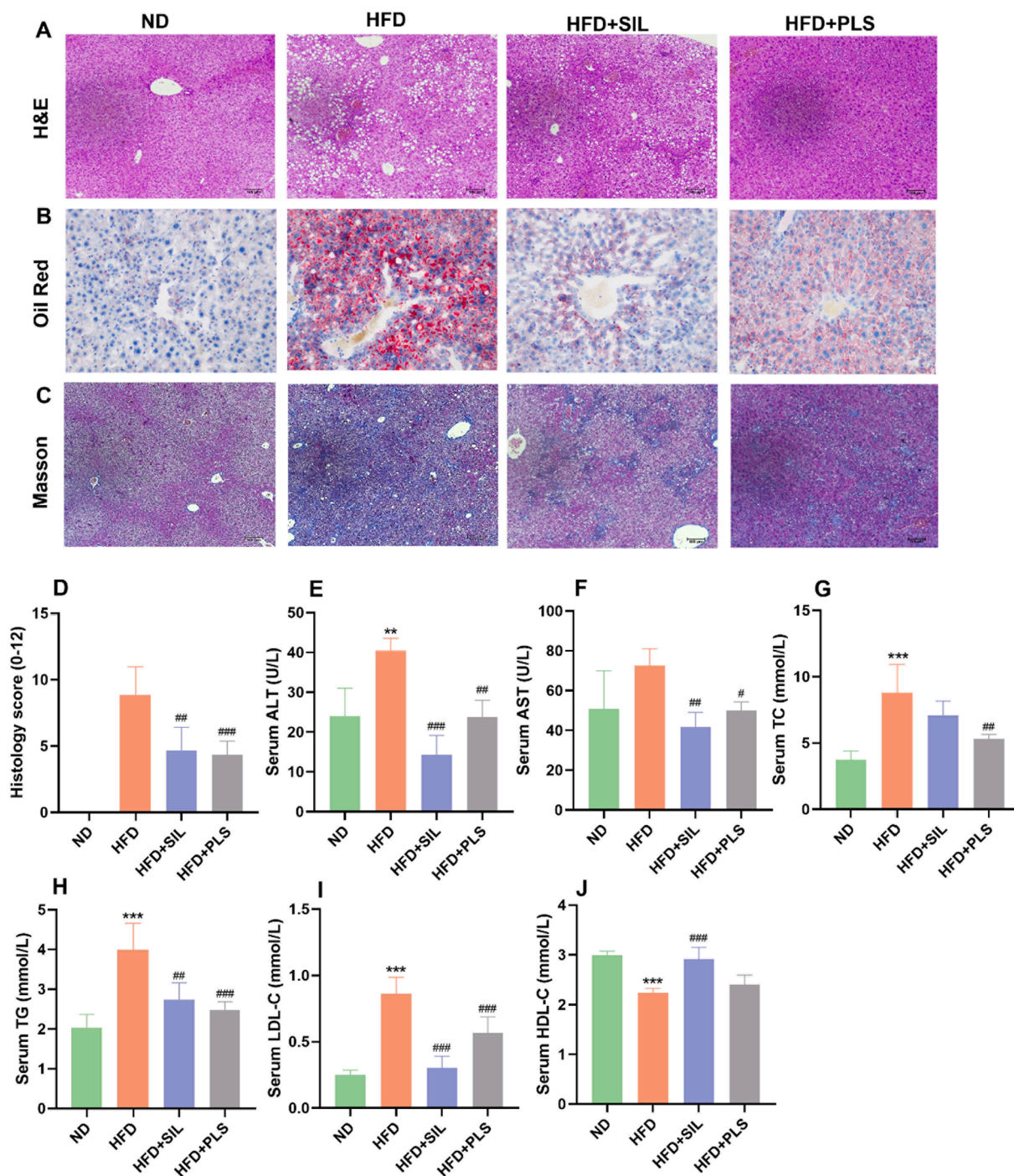


**Fig. 4.** PLS alleviated hepatic steatosis and dyslipidemia in HFD-induced NAFLD. (A) H&E staining of liver sections. (B) Oil-red staining of liver sections. (C) Masson's trichrome staining of liver sections. (D) Histology scores based on H&E, Oil Red and Masson's trichrome staining. (E) Serum ALT level. (F) Serum AST level. (G) Serum TC level. (H) Serum TG level. (I) Serum LDL level. (J) Serum HDL level. \*\*  $p < 0.01$ , \*\*\*  $p < 0.001$ , vs. ND group. #  $p < 0.05$ , ##  $p < 0.01$ , ###  $p < 0.001$ , vs. HFD group.

### 3.4. PLS improved HFD-induced gut dysbiosis in NAFLD mice

#### 3.4.1. Regulation of gut microbial composition

Since PLS displayed a role in regulating gut microbiota *in vitro*, here we further investigated the influence of PLS on HFD-induced dysbiosis in mice.

The overall microbial structure was analyzed by examining alpha-diversity (via Sobs and Shannon indices) and beta-diversity (via PCoA analysis). HFD-feeding led to decreased Sobs and unchanged Shannon index, indicating reduced microbial richness (Fig. 5A-B). PCoA analysis

based on ASV level showed that HFD-induced NAFLD mice had a remarkable shift in fecal microbial structure (Fig. 5C). However, PLS treatment recovered HFD-induced reduction of Sobs index (Fig. 5A). Besides, PLS mediated microbial structural alterations in NAFLD mice as specimens from HFD and HFD + PLS groups were well separated in PCoA plot (Fig. 5C). Treatment with PLS shifted the HFD-induced microbial variations and showed a tendency to close toward ND group on the PC1 axis (Fig. 5C), indicating PLS may at least partially recover HFD-mediated microbial changes. The results demonstrated that PLS may in part recover HFD-induced gut microbe structure alteration.

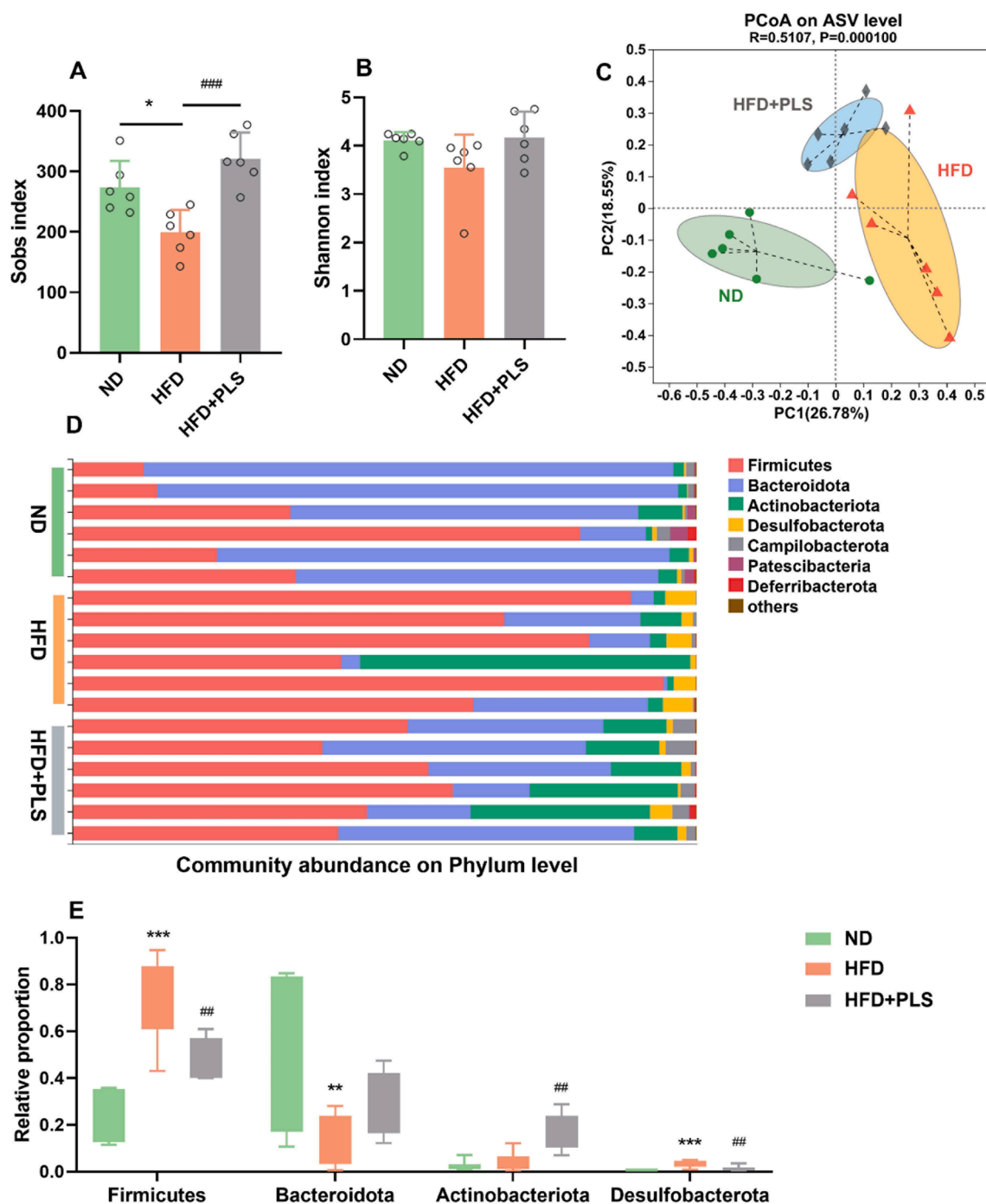


**Fig. 5.** PLS modulated gut microbial diversity and structure in HFD-induced NAFLD. (A) Sobs index. (B) Shannon index. (C) PCoA analysis based on ASV level. (D) Community abundance on phylum level. (E) Relative abundance of phyla of Firmicutes, Bacteroidota, Actinobacteriota and Desulfobacterota. \*\*  $p < 0.01$ , \*\*\*  $p < 0.001$ , vs ND group. #  $p < 0.05$ , ##  $p < 0.01$ , vs HFD group.

### 3.4.2. Key gut microbes responded to PLS

At phylum level, there were considerable changes in NAFLD mice and those treated with PLS when compared to ND mice (Fig. 5D). The abundance of Firmicutes was prominently increased ( $p < 0.001$ ) from  $23.77 \pm 11.44\%$  (ND group) to  $72.26 \pm 16.92\%$  (HFD group), which was then distinctly decreased ( $p < 0.01$ ) to  $48.75 \pm 8.50\%$  (HFD + PLS group) (Fig. 5D). However, the abundance of Bacteroidota was significantly decreased ( $p < 0.01$ ) from  $54.62 \pm 30.07\%$  (ND group) to  $13.98 \pm 10.93\%$  (HFD group), which was increased upon PLS intervention to  $30.67 \pm 12.79\%$  (Fig. 5D). Besides, HFD-feeding significantly promoted ( $p < 0.001$ ) the proportion of Desulfobacterota which was notably

reversed by PLS treatment (Fig. 5D). Although HFD did not alter Actinobacteriota, PLS significantly increased its abundance ( $p < 0.01$ ) (Fig. 5D). It has been reported that obesity and NAFLD was associated with the increased abundance of Firmicutes and decreased abundance of Bacteroidota in gut (Ley et al., 2005). Actinobacteriota contained both beneficial bacteria (such as *Bifidobacterium spp.*) and harmful ones. Thus, the results demonstrated that PLS attenuated HFD-induced dysbiosis (increased Firmicutes and Desulfobacterota, and decreased Bacteroidota) at phylum level and increased Actinobacteriota level.

To further identify the changes of specific microbes at genus level with PLS treatment, LefSe (LDA score  $> 4$ ) was performed (Fig. 6A). The

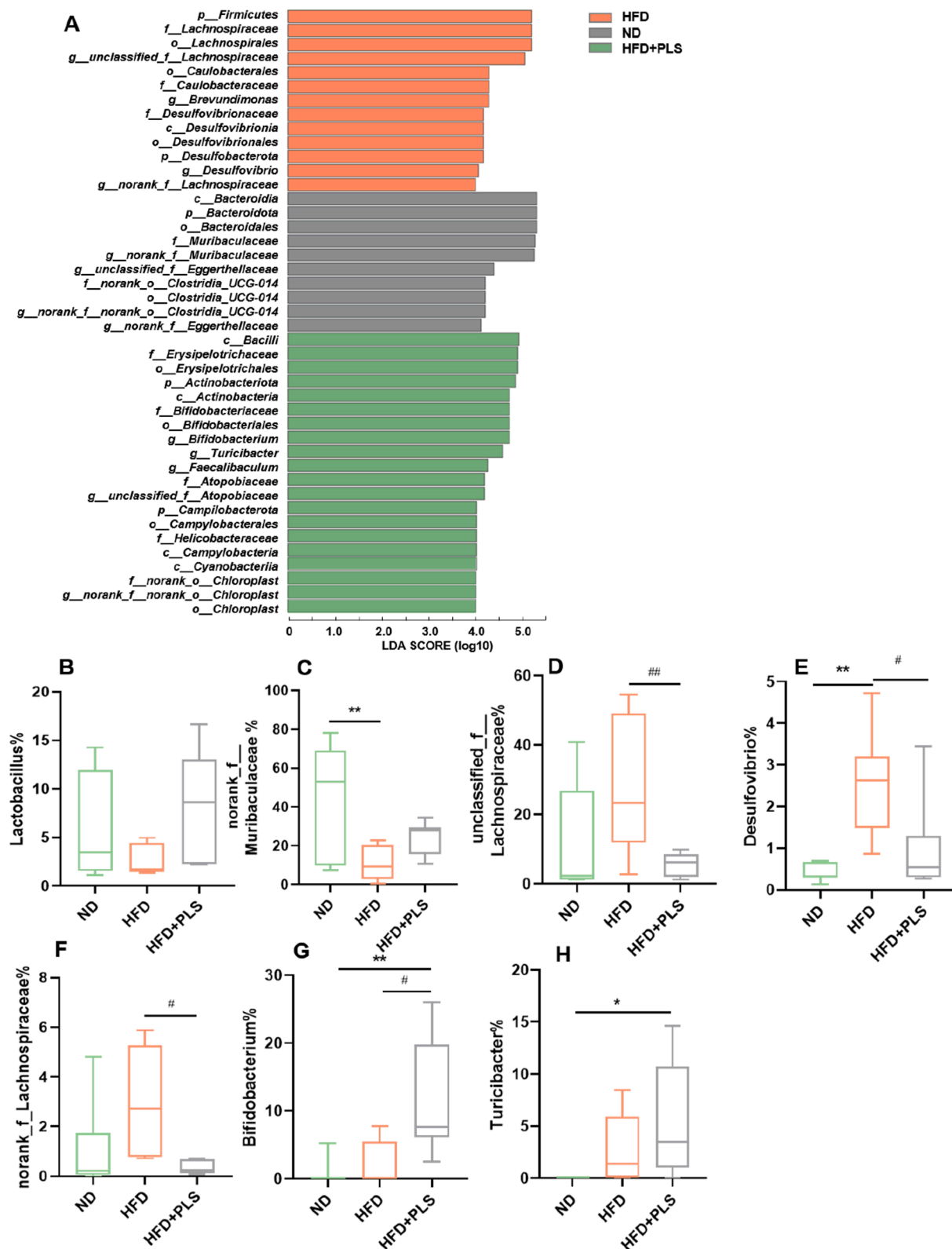


Fig. 6. Identification of key microbial changes at genus level after PLS intervention. (A) Cladogram of LefSe analysis. Relative abundance of (B) *Lactobacillus*, (C) *norank\_f\_Muribaculaceae*, (D) *unclassified\_f\_Lachnospiraceae*, (E) *Desulfovibrio*, (F) *norank\_f\_Lachnospiraceae*, (G) *Bifidobacterium*, and (H) *Turicibacter*. \*  $p < 0.05$ , \*\*  $p < 0.01$ , \*\*\*  $p < 0.001$ , vs. ND group. #  $p < 0.05$ , ##  $p < 0.01$ , vs. HFD group.

plot (Fig. 6A) showed that Firmicutes and Desulfovacterota bacteria including *unclassified\_f\_Lachnospiraceae*, *Desulfovibrio* and *norank\_f\_Lachnospiraceae* were enriched in HFD group. Abundant microbial genus in ND group included *norank\_f\_Muribaculaceae* and

*norank\_f\_norank\_o\_Clostridia\_UCG-014* in Bacteroidota. After PLS treatment in NAFLD mice, several genera in Actinobacteriota such as *Bifidobacterium*, and *Turicibacter* were enriched. Specifically, the abundance of *Lactobacillus* (Fig. 6B) and *norank\_f\_Muribaculaceae* (Fig. 6C) was

decreased in HFD group compared to ND group, and there was an obvious increase of these bacteria upon PLS treatment although no statistical difference. Furthermore, the abundance of *unclassified\_f\_Lachnospiraceae* (Fig. 6D), *Desulfovibrio* (Fig. 6E) and *norank\_f\_Lachnospiraceae* (Fig. 6F) were increased in HFD group, which was further decreased in HFD + PLS group to the level comparable to that in ND group. Notably, the abundance of *Bifidobacterium* (Fig. 6G) and *Turicibacter* (Fig. 6H) were not changed in HFD group, but had a significant increase in HFD + PLS group, which might be PLS-specific bacteria. The above results suggested that HFD-induced microbial changes were at least partially recovered by PLS treatment and there were certain bacteria specifically in response to PLS.

*Lactobacillus* as probiotics could protect against hepatic steatosis by reducing fatty acid absorption in gut (Jang et al., 2019) and prevent gut epithelial from oxidative damage (Jones et al., 2013). *Bifidobacterium* was another important probiotics that were beneficial microbes for inflammatory bowel disease and colorectal cancer (Le Leu, Hu, Brown, Woodman, & Young, 2010; Le et al., 2014). *Turicibacter* was positively correlated with butyrate production (Zheng, Wang, Wang, Chen, & Zhou, 2020). In contrast, *Desulfovibrio* was considered to be harmful bacteria, which had been suggested to be enriched in HFD-fed NAFLD mice and contribute to gut inflammation (Carbonero et al., 2012; Mukhopadhyaya et al., 2012; Wang et al., 2020). Based on these documented information, PLS treatment could help to recover gut dysbiosis and maintain intestinal health in NAFLD mice via increasing potentially beneficial bacteria and inhibiting harmful ones. As described in early sections, PLS fermentation *in vitro* led to enriched *Lactobacillus* and reduced *Desulfovibrio*, which was generally consistent with the findings in NAFLD mice. Moreover, *Bifidobacterium* and *Turicibacter* might be another important feature for PLS treatment in NAFLD mice.

### 3.5. PLS increased SCFA production in NAFLD mice

The production of SCFAs (Fig. 7) including acetic acid, butyric acid, propionic acid, valeric acid, isobutyric acid, isovaleric acid, and hexanoic acid was further determined in the fecal sample of NAFLD mice. The results showed that PLS supplementation reversed HFD-diet induced decrease of acetic acid, butyric acid and propionic acid in mice, although there was no statistical difference for acetic acid and propionic acid. This result was generally in line with the *in vitro* fermentation. PLS had no significant effect on other SCFAs in NAFLD mice. As a result, the total SCFA production in HFD+PLS group was elevated compared to the HFD group.

SCFAs are major fermentation metabolites of the gut microbiota and play considerable roles in colonic health and integrity (Íñiguez-Gutiérrez et al., 2020). Recent studies have demonstrated that the decreased production of SCFAs, especially butyrate, resulted in increased gut permeability, endotoxemia and systemic inflammation (Chen & Vitetta, 2020). Moreover, SCFAs are necessary energy sources for gut microbiota and colonocytes which are critical for maintaining gut homeostasis. In our study, PLS enriched the specific bacteria population of *Lactobacillus in vitro* and elevated overall production of SCFAs (more specifically, acetic acid and butyric acid). In NAFLD mice, PLS supplementation increased the abundance of bacteria of *Lactobacillus*, *Bifidobacterium* and *Turicibacter*, along with increased contents of butyric acid and total SCFAs. Previous reports have showed that some strains of *Lactobacillus* and *Bifidobacterium* promoted the production of acetic acid, butyric acid, and valeric acid (Yao, Cao, Zhang, Kwok, Zhang, & Zhang, 2021; Horiuchi, 2020). The results here thus indicated that PLS regulated gut microbiota composition to promote SCFAs production in NAFLD mice which might contribute to the alleviation of metabolic disorder.

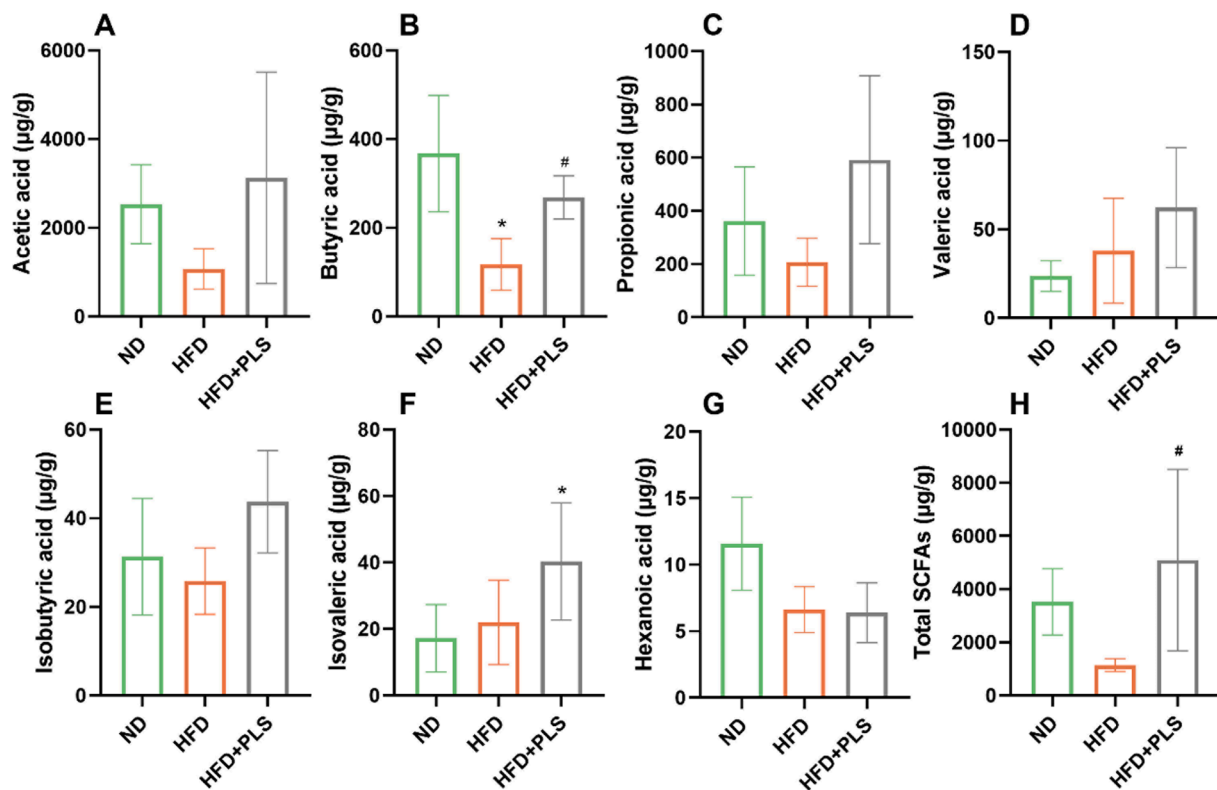


Fig. 7. Production of SCFAs in colonic contents after PLS treatment in NAFLD mice. The amounts ( $\mu\text{g/g}$ ) of (A) acetic acid, (B) butanoic acid, (C) propanoic acid, (D) valeric acid, (E) iso-butyric acid, (F) isovaleric acid, and (G) hexanoic acid. (H) The total amounts ( $\mu\text{g/g}$ ) of SCFAs. \*  $p < 0.05$ , vs. ND group. #  $p < 0.05$ , vs. HFD group.

### 3.6. Alleviation of NAFLD by PLS was correlated with specific gut microbial changes

Furthermore, a correlation analysis based on db-RDA and Pearson's correlation were performed. The db-RDA results (Fig. 8A) demonstrated that ND mice were positively correlated with higher HDL-C, enriched *norank\_Muribaculaceae*, whereas the HFD-induced NAFLD mice were positively associated with increased LDL-C, AST/ALT, histology score, inflammation (TNF- $\alpha$  and IL-6) and TG/TC, enriched *Desulfovibrio*, *Lachnospiraceae\_NK4A136\_group* and *unclassified\_f\_Lachnospiraceae*. Notably, PLS treatment evidently shifted the microbiome distribution of NAFLD mice, and the HFD + PLS group was moved towards to the ND mice along CAP1 axis, which enriched with *Lactobacillus*, *Bifidobacterium* and *Turicibacter*, and showed increased SCFAs. Moreover, the Pearson's correlation heatmap (Fig. 8B) further demonstrated that the higher inflammation (TNF- $\alpha$  and IL-6 level), histology score, AST/ALT, TG/TC and LDL-C was positively correlated with *unclassified\_f\_Lachnospiraceae*, *Desulfovibrio* and *norank\_f\_Lachnospiraceae*, and was negatively correlated with *Lactobacillus*, *norank\_f\_Muribaculaceae* and *Turicibacter*. Meanwhile, the increased HDL-C and SCFA was positively correlated with *Lactobacillus*, *norank\_Muribaculaceae* and *Bifidobacterium*. It is

suggested that the regulation of PLS on gut microbiome played a considerable role in protecting against HFD-induced NAFLD.

### 3.7. Structure-function relationship

It was demonstrated in the present study that PLS significantly regulated gut microbiota and alleviated NAFLD in mice. The modulated intestinal microbial structure and improved inflammation, hepatic steatosis and dyslipidemia by PLS might be associated with its prebiotic properties as mediated by its inherent and distinct physicochemical properties. A smoother on the granule surface, larger particle size, lower branching degree and higher degree of crystallization of PLS may lead to poor digestibility of the starch granule according to previous literatures (Gaenssle et al., 2021; Guo et al., 2017). Besides, PLS with type-B or type-C crystallites made it generally more resistant to amylolytic digestion. Generally, the B- or C-type starch showed more resistance to enzyme hydrolysis than that of A-type (Wei et al., 2010), and the B-type polymorphs were responsible for anti-digestibility of C-type starches (Huang, Lin, Wang, Wang, Liu, & Wei, 2016). Furthermore, PLS with certain proportions of RS ( $23.14 \pm 0.36\%$ ) and large slowly digestible starches, which contributed to proliferation of specific gut microbiota

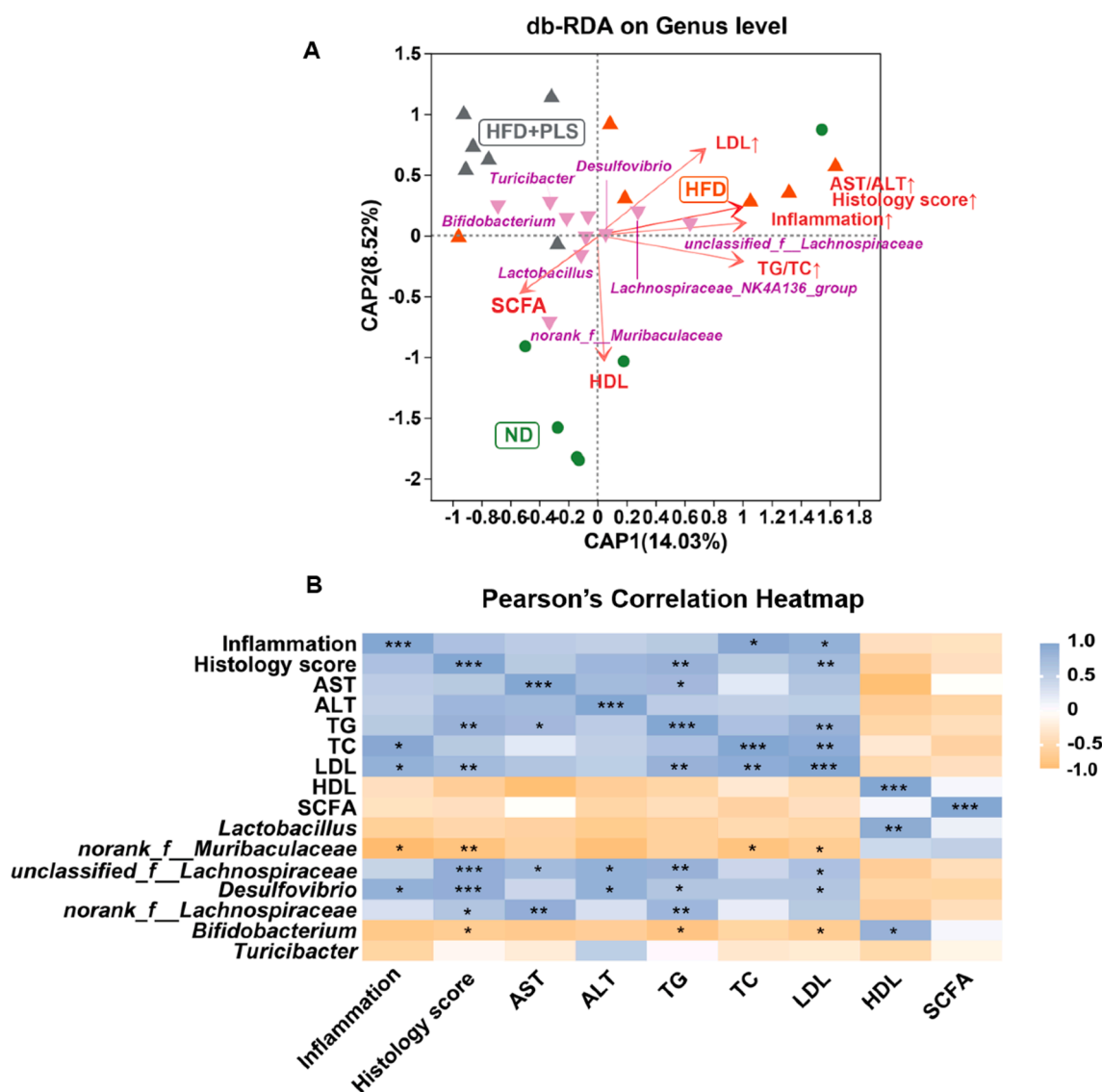


Fig. 8. Distance-based redundancy analysis (db-RDA) analysis and Pearson's correlation analysis on association of key microbial changes and main pathological abnormalities in response to PLS treatment. (A) db-RDA analysis. (B) Pearson's correlation heatmap.

(Guo et al., 2017). Previous study has been reported that fermentation of RS had a key impact on reshaping the gut microbial composition that contributed to produce starch-degrading enzymes and promoted the production of intestinal SCFAs, which prevented metabolic disease such as T2DM and obesity (Liu et al., 2020). Interestingly, PLS enriched different SCFAs-producing bacteria, which were host-beneficial bacteria in NAFLD mice in our research, such as *Lactobacillus*, *Bifidobacterium* and *Turicibacter*. Besides, PLS exhibited gut microbiota regulation by reducing opportunistic harmful gut microbe, especially *Desulfovibrio*. It is assumed that a slow and steady fermentation rate of PLS could result in a stable production rate of SCFAs in the colon. Consequently, it led to a more favorable microenvironment in the intestine for gut microbiome to gain energy, which further contributed to a satisfactory reaction between gut microbiota and host.

#### 4. Conclusion

In this study, the *P. lobata* starch was structurally and physicochemically characterized via analysis of micromorphology, RS and amylose content, molecular weight distribution, branching degree, CLD, FT-IR spectrum, water solubility, swelling power and pasting property. Furthermore, *in vitro* fermentation of PLS resulted in specifically altered composition of gut microbiota and increased SCFAs production, showing a potential prebiotic effect. Moreover, PLS could alleviate inflammation, hepatic steatosis and dyslipidemia in NAFLD mice, and ameliorate HFD-mediated gut dysbiosis. This study for the first time characterized the PLS, and suggested that PLS can be used as a prebiotic for the prevention and treatment HFD-induced NAFLD.

#### CRedit authorship contribution statement

**Yifei Yang:** Investigation, Validation, Formal analysis, Writing – original draft, Visualization, Writing – review & editing. **Mingxing Li:** Investigation, Validation, Formal analysis, Writing – original draft, Visualization. **Qin Wang:** Investigation, Validation, Formal analysis, Writing – original draft, Visualization. **Huimin Huang:** Investigation, Validation, Visualization. **Yueshui Zhao:** Writing – review & editing. **Fukuan Du:** Writing – review & editing. **Yu Chen:** Writing – review & editing. **Jing Shen:** Writing – review & editing. **Haomin Luo:** Writing – review & editing. **Qianyun Zhao:** Validation, Writing – review & editing. **Jiuping Zeng:** Validation, Writing – review & editing. **Wanping Li:** Validation, Writing – review & editing. **Meijuan Chen:** Validation, Writing – review & editing. **Xiaobing Li:** Validation, Writing – review & editing. **Fang Wang:** Validation, Writing – review & editing. **Yuhong Sun:** Validation, Writing – review & editing. **Li Gu:** Validation, Writing – review & editing. **Zhangang Xiao:** Writing – review & editing, Project administration, Funding acquisition. **Xu Wu:** Conceptualization, Methodology, Formal analysis, Writing – original draft, Writing – review & editing, Project administration, Funding acquisition.

#### Declaration of Competing Interest

The authors declare that they have no known competing financial interests or personal relationships that could have appeared to influence the work reported in this paper.

#### Acknowledgement

This work is supported by grants from Science and Technology Program of Luzhou, China (No. 21CGZHPT0001), and Southwest Medical University (No. 2021ZKZD017).

#### Appendix A. Supplementary data

Supplementary data to this article can be found online at <https://doi.org/10.1016/j.foodres.2022.111401>.

#### References

- Broekaert, W. F., Courtin, C. M., Verbeke, K., Van de Wiele, T., Verstraete, W., & Delcour, J. A. (2011). Prebiotic and other health-related effects of cereal-derived arabinoxylans, arabinoxylan-oligosaccharides, and xylooligosaccharides. *Critical Reviews in Food Science and Nutrition*, 51(2), 178–194.
- Cai, C., Lin, L., Man, J., Zhao, L., Wang, Z., & Wei, C. (2014). Different structural properties of high-amylose maize starch fractions varying in granule size. *Journal of Agriculture and Food Chemistry*, 62(48), 11711–11721.
- Carbonero, F., Benefiel, A. C., Alizadeh-Ghamsari, A. H., & Gaskins, H. R. (2012). Microbial pathways in colonic sulfur metabolism and links with health and disease. In *Frontiers in Physiology* (Vol. 3, pp. 448).
- Chen, B., Dang, L., Zhang, X., Fang, W., Hou, M., Liu, T., & Wang, Z. (2017). Physicochemical properties and micro-structural characteristics in starch from kudzu root as affected by cross-linking. *Food Chemistry*, 219, 93–101.
- Chen, J., & Vitetta, L. (2020). Gut Microbiota Metabolites in NAFLD Pathogenesis and Therapeutic Implications. *International Journal of Molecular Sciences*, 21(15).
- Chen, X., Yu, J., & Shi, J. (2018). Management of Diabetes Mellitus with Puerarin, a Natural Isoflavone From *Pueraria lobata*. *American Journal of Chinese Medicine*, 46(8), 1771–1789.
- Eerlingen, R., Decuninck, M., & Delcour, J. (1993). Enzyme resistant starch 11. Influence of amylose chain length on resistant starch and formation. *Cereal Chemistry*, 70(3), 345–350.
- Gaenssle, A. L. O., Satyawati, C. A., Xiang, G., van der Maarel, M., & Jurak, E. (2021). Long chains and crystallinity govern the enzymatic degradability of gelatinized starches from conventional and new sources. *Carbohydrate Polymers*, 260, 117801.
- Genkina, N. K., Wikman, J., Bertoft, E., & Yuryev, V. P. (2007). Effects of structural imperfection on gelatinization characteristics of amylopectin starches with A- and B-type crystallinity. *Biomacromolecules*, 8(7), 2329–2335.
- Gidley, M. J., Cooke, D., Darke, A., Hoffmann, R., Russell, A., & Greenwell, P. (1995). Molecular order and structure in enzyme-resistant retrograded starch. *Carbohydrate Polymers*, 28(1), 23–31.
- Guo, Z., Jia, X., Zhao, B., Zeng, S., Xiao, J., & Zheng, B. (2017). C-type starches and their derivatives: Structure and function. *Annals of the New York Academy of Sciences*, 1398(1), 47–61.
- Han, R., Ma, J., & Li, H. (2018). Mechanistic and therapeutic advances in non-alcoholic fatty liver disease by targeting the gut microbiota. *Front Med*, 12(6), 645–657.
- Hanashiro, I., Abe, J.-I., & Hizukuri, S. (1996). A periodic distribution of the chain length of amylopectin as revealed by high-performance anion-exchange chromatography. *Carbohydrate Research*, 283, 151–159.
- Horiuchi, H., Kamikado, K., Aoki, R., Suganuma, N., Nishijima, T., Nakatani, A., & Kimura, I. (2020). *Bifidobacterium animalis* subsp. *lactis* GCL2505 modulates host energy metabolism via the short-chain fatty acid receptor GPR43. *Scientific Reports*, 10(1), 4158.
- Hu, J., Lin, S., Zheng, B., & Cheung, P. C. K. (2018). Short-chain fatty acids in control of energy metabolism. *Critical Reviews in Food Science and Nutrition*, 58(8), 1243–1249.
- Íñiguez-Gutiérrez, L., Godínez-Méndez, L. A., Fafutis-Morris, M., Padilla-Arellano, J. R., Corona-Rivera, A., Bueno-Topete, M. R., Rojas-Rejón Ó, A., & Delgado-Rizo, V. (2020). Physiological concentrations of short-chain fatty acids induce the formation of neutrophil extracellular traps *in vitro*. *Int J Immunopathol Pharmacol*, 34, 2058738420958949.
- Jang, H. R., Park, H. J., Kang, D., Chung, H., Nam, M. H., Lee, Y., ... Lee, H. Y. (2019). A protective mechanism of probiotic *Lactobacillus* against hepatic steatosis via reducing host intestinal fatty acid absorption. *Experimental & Molecular Medicine*, 51(8), 1–14.
- Jeon, Y. D., Lee, J. H., Lee, Y. M., & Kim, D. K. (2020). Puerarin inhibits inflammation and oxidative stress in dextran sulfate sodium-induced colitis mice model. *Biomedicine & Pharmacotherapy*, 124, 109847.
- Jones, R. M., Luo, L., Ardita, C. S., Richardson, A. N., Kwon, Y. M., Mercante, J. W., ... Neish, A. S. (2013). Symbiotic lactobacilli stimulate gut epithelial proliferation via Nox-mediated generation of reactive oxygen species. *EMBO Journal*, 32(23), 3017–3028.
- Huang, J., Lin, L., Wang, J., Wang, Z., Liu, Q., & Wei, C. (2016). *In vitro* digestion properties of heterogeneous starch granules from high-amylose rice. *Food Hydrocolloids*, 54, 10–22.
- Jung, A., Chen, L. R., Suyemoto, M. M., Barnes, H. J., & Borst, L. B. (2018). A Review of *Enterococcus cecorum* Infection in Poultry. *Avian Diseases*, 62(3), 261–271.
- Kapoor, S. (2013). Anti-neoplastic effects of puerarin in systemic malignancies besides colon carcinomas. *International Journal of Pharmaceutics*, 443(1–2), 306.
- Keku, T. O., Dulal, S., Deveaux, A., Jovov, B., & Han, X. (2015). The gastrointestinal microbiota and colorectal cancer. *American Journal of Physiology. Gastrointestinal and Liver Physiology*, 308(5), G351–G363.
- Le Leu, R. K., Hu, Y., Brown, I. L., Woodman, R. J., & Young, G. P. (2010). Symbiotic intervention of *Bifidobacterium lactis* and resistant starch protects against colorectal cancer development in rats. *Carcinogenesis*, 31(2), 246–251.
- Le, T. K., Hosaka, T., Le, T. T., Nguyen, T. G., Tran, Q. B., Le, T. H., & Pham, X. D. (2014). Oral administration of *Bifidobacterium* spp. improves insulin resistance, induces adiponectin, and prevents inflammatory adipokine expressions. *Biomedical Research*, 35(5), 303–310.
- Ley, R. E., Backhed, F., Turnbaugh, P., Lozupone, C. A., Knight, R. D., & Gordon, J. I. (2005). Obesity alters gut microbial ecology. *Proc Natl Acad Sci U S A*, 102(31), 11070–11075.
- Liu, H., Zhang, M., Ma, Q., Tian, B., Nie, C., Chen, Z., & Li, J. (2020). Health beneficial effects of resistant starch on diabetes and obesity via regulation of gut microbiota: A review. *Food & Function*, 11(7), 5749–5767.

- Lozupone, C. A., Hamady, M., Cantarel, B. L., Coutinho, P. M., Henrissat, B., Gordon, J. I., & Knight, R. (2008). The convergence of carbohydrate active gene repertoires in human gut microbes. *Proceedings of the National Academy of Sciences of the United States of America*, 105(39), 15076–15081.
- Ma, Z., & Boye, J. I. (2018). Research advances on structural characterization of resistant starch and its structure-physiological function relationship: A review. *Critical Reviews in Food Science and Nutrition*, 58(7), 1059–1083.
- Maslowski, K. M., & Mackay, C. R. (2011). Diet, gut microbiota and immune responses. *Nature Immunology*, 12(1), 5–9.
- Mukhopadhyay, I., Hansen, R., El-Omar, E. M., & Hold, G. L. (2012). IBD-what role do Proteobacteria play? *Nature Reviews Gastroenterology & Hepatology*, 9(4), 219–230.
- Reddy, C. K., Luan, F., & Xu, B. (2017). Morphology, crystallinity, pasting, thermal and quality characteristics of starches from adzuki bean (*Vigna angularis* L.) and edible kudzu (*Pueraria thomsonii* Benth). *International Journal of Biological Macromolecules*, 105(Pt 1), 354–362.
- Ríos-Covián, D., Ruas-Madiedo, P., Margolles, A., Gueimonde, M., de Los Reyes-Gavilán, C. G., & Salazar, N. (2016). Intestinal Short Chain Fatty Acids and their Link with Diet and Human Health. *Frontiers in Microbiology*, 7, 185.
- Sang, Y., Bean, S., Seib, P. A., Pedersen, J., & Shi, Y. C. (2008). Structure and functional properties of sorghum starches differing in amylose content. *Journal of Agriculture and Food Chemistry*, 56(15), 6680–6685.
- Schnabl, B., & Brenner, D. A. (2014). Interactions between the intestinal microbiome and liver diseases. *Gastroenterology*, 146(6), 1513–1524.
- Sevenou, O., Hill, S. E., Farhat, I. A., & Mitchell, J. R. (2002). Organisation of the external region of the starch granule as determined by infrared spectroscopy. *International Journal of Biological Macromolecules*, 31(1–3), 79–85.
- Shi, M., Chen, Y., Yu, S., & Gao, Q. (2013). Preparation and properties of RS III from waxy maize starch with pullulanase. *Food Hydrocolloids*, 33(1), 19–25.
- Shin, N. R., Whon, T. W., & Bae, J. W. (2015). Proteobacteria: Microbial signature of dysbiosis in gut microbiota. *Trends in Biotechnology*, 33(9), 496–503.
- Singh, N., Inouchi, N., & Nishinari, K. (2006). Structural, thermal and viscoelastic characteristics of starches separated from normal, sugary and waxy maize. *Food Hydrocolloids*, 20(6), 923–935.
- Smith, P. M., Howitt, M. R., Panikov, N., Michaud, M., Gallini, C. A., Bohlooly, Y. M., ... Garrett, W. S. (2013). The microbial metabolites, short-chain fatty acids, regulate colonic Treg cell homeostasis. *Science*, 341(6145), 569–573.
- Smits, A. L. M., Ruhnau, F. C., Vliegenthart, J. F. G., & van Soest, J. J. G. (1998). Ageing of starch based systems as observed with FT-IR and solid state NM spectroscopy. *Starch*, 50, 478–483.
- Song, X., Dong, H., Zang, Z., Wu, W., Zhu, W., Zhang, H., & Guan, Y. (2021). Kudzu Resistant Starch: An Effective Regulator of Type 2 Diabetes Mellitus. *Oxidative Medicine and Cellular Longevity*, 2021, 4448048.
- Sonnenburg, E. D., Zheng, H., Joglekar, P., Higginbottom, S. K., Firbank, S. J., Bolam, D. N., & Sonnenburg, J. L. (2010). Specificity of polysaccharide use in intestinal bacteroides species determines diet-induced microbiota alterations. *Cell*, 141(7), 1241–1252.
- Van Hung, P., & Morita, N. (2007). Chemical compositions, fine structure and physicochemical properties of kudzu (*Pueraria lobata*) starches from different regions. *Food Chemistry*, 105(2), 749–755.
- Vester-Andersen, M. K., Mirsepasi-Lauridsen, H. C., Prossberg, M. V., Mortensen, C. O., Trager, C., Skovsen, K., ... Petersen, A. M. (2019). Increased abundance of proteobacteria in aggressive Crohn's disease seven years after diagnosis. *Scientific Reports*, 9(1), 13473.
- Wang, J. W., Wang, H. D., Cong, Z. X., Zhou, X. M., Xu, J. G., Jia, Y., & Ding, Y. (2014). Puerarin ameliorates oxidative stress in a rodent model of traumatic brain injury. *Journal of Surgical Research*, 186(1), 328–337.
- Wang, P., Wang, J., Li, D., Ke, W., Chen, F., & Hu, X. (2020). Targeting the gut microbiota with resveratrol: A demonstration of novel evidence for the management of hepatic steatosis. *Journal of Nutritional Biochemistry*, 81, Article 108363.
- Wang, Y., Dillidaxi, D., Wu, Y., Sailike, J., Sun, X., & Nabi, X. H. (2020). Composite probiotics alleviate type 2 diabetes by regulating intestinal microbiota and inducing GLP-1 secretion in db/db mice. *Biomedicine & Pharmacotherapy*, 125, 109914.
- Wei, C., Xu, B., Qin, F., Yu, H., Chen, C., Meng, X., ... Liu, Q. (2010). C-type starch from high-amylose rice resistant starch granules modified by antisense RNA inhibition of starch branching enzyme. *Journal of Agriculture and Food Chemistry*, 58(12), 7383–7388.
- Wong, K. H., Li, G. Q., Li, K. M., Razmovski-Naumovski, V., & Chan, K. (2011). Kudzu root: Traditional uses and potential medicinal benefits in diabetes and cardiovascular diseases. *Journal of Ethnopharmacology*, 134(3), 584–607.
- Xu, J., Chen, N., Wu, Z., Song, Y., Zhang, Y., Wu, N., ... Liu, Y. (2018). 5-Aminosalicylic Acid Alters the Gut Bacterial Microbiota in Patients With Ulcerative Colitis. *Frontiers in Microbiology*, 9, 1274.
- Yao, G., Cao, C., Zhang, M., Kwok, L. Y., Zhang, H., & Zhang, W. (2021). *Lactobacillus casei* Zhang exerts probiotic effects to antibiotic-treated rats. *Computational and Structural Biotechnology Journal*, 19, 5888–5897.
- Yan, Z., Fan, R., Yin, S., Zhao, X., Liu, J., Li, L., ... Ge, L. (2015). Protective effects of Ginkgo biloba leaf polysaccharide on nonalcoholic fatty liver disease and its mechanisms. *International Journal of Biological Macromolecules*, 80, 573–580.
- Yang, X., Mo, W., Zheng, C., Li, W., Tang, J., & Wu, X. (2020). Alleviating effects of noni fruit polysaccharide on hepatic oxidative stress and inflammation in rats under a high-fat diet and its possible mechanisms. *Food & Function*, 11(4), 2953–2968.
- Yin, J., Ren, W., Wei, B., Huang, H., Li, M., Wu, X., ... Wang, Y. (2020). Characterization of chemical composition and prebiotic effect of a dietary medicinal plant *Penthorum chinense* Pursh. *Food Chemistry*, 319, 126568.
- Younossi, Z. M., Koenig, A. B., Abdelatif, D., Fazel, Y., Henry, L., & Wymer, M. (2016). Global epidemiology of nonalcoholic fatty liver disease-Meta-analytic assessment of prevalence, incidence, and outcomes. *Hepatology*, 64(1), 73–84.
- Zeng, F., Li, T., Zhao, H., Chen, H., Yu, X., & Liu, B. (2019). Effect of debranching and temperature-cycled crystallization on the physicochemical properties of kudzu (*Pueraria lobata*) resistant starch. *International Journal of Biological Macromolecules*, 129, 1148–1154.
- Zhang, C., Qiu, M., Wang, T., Luo, L., Xu, W., Wu, J., ... Wang, X. (2021). Preparation, structure characterization, and specific gut microbiota properties related to anti-hyperlipidemic action of type 3 resistant starch from *Canna edulis*. *Food Chemistry*, 351, 129340.
- Zheng, B., Wang, T., Wang, H., Chen, L., & Zhou, Z. (2020). Studies on nutritional intervention of rice starch-oleic acid complex (resistant starch type V) in rats fed by high-fat diet. *Carbohydrate Polymers*, 246, 116637.
- Zhong, F., Li, Y., Ibáñez, A. M., Oh, M. H., McKenzie, K. S., & Shoemaker, C. (2009). The effect of rice variety and starch isolation method on the pasting and rheological properties of rice starch pastes. *Food Hydrocolloids*, 23, 406–414.
- Zhu, L., Xue, J., Xia, Q., Fu, P. P., & Lin, G. (2017). The long persistence of pyrrolizidine alkaloid-derived DNA adducts in vivo: Kinetic study following single and multiple exposures in male ICR mice. *Archives of Toxicology*, 91(2), 949–965.